Phonon ballistic transport and Anderson localization in Si$_{1-x}$Ge$_x$ alloyed nanowires

Wei Zhang,[1,2] Yangyu Guo [ID],[1,2] Shi-Yun Xiong,[3,*] and Hong-Liang Yi [ID][1,2,†]

[1]*School of Energy Science and Engineering, Harbin Institute of Technology,*
Harbin 150001, People's Republic of China
[2]*Key Laboratory of Aerospace Thermophysics, Ministry of Industry and Information Technology,*
Harbin 150001, People's Republic of China
[3]*Guangzhou Key Laboratory of Low-Dimensional Materials and Energy Storage Devices, School of Materials and Energy,*
Guangdong University of Technology, Guangzhou 510006, People's Republic of China

Heat transport plays a crucial role in various applications such as waste energy harvesting, thermal barrier coatings, and heat dissipation in microelectronics. In this paper, the frequency-dependent heat transport characteristics in mass disordered Si$_{1-x}$Ge$_x$ nanowires (NWs) are investigated based on the nonequilibrium Green's function method. The results demonstrate the coexistence of phonons with ballistic transport, diffusive transport, and Anderson localization in SiGe alloyed NWs. Ballistic phonons are observed at low frequencies, with a NW length of up to 2 μm and Ge concentrations ranging from 1 to 50%. As the Ge concentration increases, the upper frequency limit for ballistic transport shifts to lower frequencies. However, the thermal conductivity contributed by these ballistic phonons increases due to enhanced scattering and localization of mid- and high-frequency phonons. Moreover, for ultralong samples, phonon localization occurs across a wide frequency range. The localization length decreases with increasing frequency, indicating that high-frequency phonons are more prone to localization in SiGe-alloyed NWs. Additionally, the localization length decreases with increasing Ge concentration, revealing a stronger localization effect in highly mass-disordered systems. Our results contribute to the understanding of heat transport in low-dimensional disordered systems and could be beneficial to guiding the design of thermoelectric materials and thermal barrier coatings.

I. INTRODUCTION

The manipulation of thermal conductivity (TC) in nanostructures, whether to reduce or increase it, has been a challenging and intriguing area of research. In recent years, various nanostructures, such as nanowires (NWs) [1–3], thin films [4–6], superlattices [7–10], periodic porous nanostructures [11–13], nanocomposites [14,15], and amorphous structures [16], have been explored for tuning heat conduction through mechanisms like phonon scattering and band folding. Unlike in an atomically periodic medium, waves encounter numerous scatterings and cannot propagate freely in disordered media [17]. Transport theory suggests that waves in disordered media exhibit different transport regimes due to interference effects: ballistic, diffusive, and localization regimes [18]. Normally, in atomically ordered systems, phonon transport behavior can be described by two observable lengths: the wavelength and the phonon mean free path [19]. When the system size is much larger than the phonon mean free path, the system displays macroscopic diffusive transport and can be described using the thermal diffusion equation. Consequently, TC is solely determined by the material properties and remains independent of system size. However, if the

characteristic size is shorter or comparable with the mean free path, the classical size effect comes into play, where phonon transport becomes quasiballistic or ballistic. In the ballistic regime, TC is linearly proportional to the characteristic size of the system [19,20]. Usually, the ballistic and diffusive transports can coexist within a system, as they depend on the modes involved. Low-frequency acoustic phonons with long wavelengths experience fewer scattering and thus possess large mean free paths, making them more prone to ballistic transport. In contrast, high-frequency phonons tend to reach the diffusive transport limit due to their relatively short mean free paths. In additional to the ballistic and diffusive transport, multiple coherent elastic scatterings in disordered systems can result in phonon Anderson localizations, which is a phenomenon described by the wave effect of phonons and commonly observed in amorphous materials [21,22] and alloys [23,24].

Mass disordered systems serve as an excellent platform for studying phonon localization due to the dominant role of elastic scattering in heat transport within such systems [25,26]. The coherent backscattering effect, which leads to localization, is fully effective only when all scatterers are elastic [17]. According to the Rayleigh scattering theory, the phonon scattering strength by atomic-scale defects is proportional to the fourth power of phonon frequencies. As the lattice imperfections in mass-disordered systems are at the atomic scales, they efficiently scatter high-frequency phonons with

*syxiong@gdut.edu.cn
†yihongliang@hit.edu.cn

short wavelengths, while they have less impact on the low-frequency phonons (acoustic modes) with long wavelengths [26]. As a result, the high-frequency phonons tend to localize more easily, whereas the low-frequency phonons may exhibit ballistic transport. Phonon localization in random disordered systems exhibit two main features: exponential reduction in phonon transmission with increasing system length [27,28] and attainment of maximum TC with increasing length [29,30]. The phonon localization effect in carbon nanotubes with isotopic disorder has been investigated by Savić *et al.* [27] and Yamamoto *et al.* [28]. However, these two studies have arrived at contrasting conclusions. Savić *et al.* [27] found that the thermal transport in isotopically doped carbon nanotubes does not exhibit localization effects [27], whereas Yamamoto *et al.* [28] discovered that the phonon transmission histogram shows a logarithmic distribution in certain frequency ranges [28], which is a character of the localization effect. Localization effects have been directly observed in experiments, where a maximum TC was identified at a particular length in nanodots embedded within periodic superlattices [29,30]. In a composition-graded Si/Ge superlattice, TC demonstrates a minimum with varying system length when there is sufficient long-range disorder [31]. In addition, broadband Andresen localization results in a sharp 98% decrease in TC at room temperature, where the mode-level localization length was directly extracted from the exponential decay of transmission functions with length [32,33]. Despite the various perspectives employed in these studies to analyze localization, the characteristics and frequency range of phonon localization in low-dimensional materials with random disordered structures remain unclear.

In contrast to bulk materials, the TC of low-dimensional materials exhibits a size dependence due to their limited nanoscale dimensions [34]. It has been observed that the TC in one-dimensional or quasi-one-dimensional nanomaterials diverges following a power-law relationship [35]. For example, Chang *et al.* [36] experimentally found that the TC of carbon nanotubes and boron nitride nanotubes diverges with length as $L^{0.6}$ and $L^{0.5}$, respectively [20,37,38]. A similar power-law divergence of TC was also observed in Si NWs with lengths up to 1.1 μm [39]. In comparison with pure Si NWs, SiGe-alloyed NWs exhibit a stronger length dependence of TC due to the severe inhibition of high-frequency phonon transport by point defects [40]. Experimentally, Hsiao *et al.* [41] reported an increase in TC with lengths for SiGe-alloyed NWs up to 8.3 um, beyond which the TC reaches a plateau. However, a recent study by Smith *et al.* [42] demonstrated that the TC of SiGe NWs remains constant between sample lengths of 2 and 10 μm. Currently, the boundary between ballistic and diffusive transport of phonons in $Si_{1-x}Ge_x$ NWs with micrometer lengths remains ambiguous.

In this paper, we investigate the phonon transport behaviors in $Si_{1-x}Ge_x$ NWs with lengths ranging from 0.5 nm to 2 μm based on the nonequilibrium Green's function (NEGF) method [43–46]. Our findings reveal that the low-frequency modes exhibit ballistic transport over long distances, demonstrating a long phonon mean free path. Despite a reduction in the frequency range of ballistic transport with increasing Ge concentration, there are still low-frequency phonons capable of traveling up to 2 μm without scattering. Moreover, we
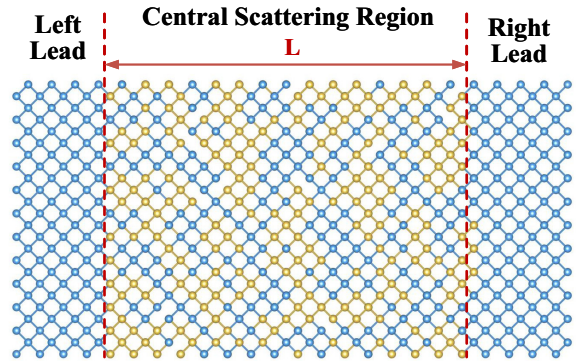
FIG. 1. Schematic illustration of the nanowire (NW) structure for the nonequilibrium Green's function (NEGF) calculation. The structure consists of the left and right leads and the central scattering region. The left and right leads are pure silicon with two conventional lattices in length, and the central scattering region is formed by SiGe-alloyed NWs with a length of *L*. The blue and yellow spheres represent Si and Ge atoms, respectively.

uncover the occurrence of Anderson localization in the mid- and high-frequency ranges, leading to a significant reduction in TC and the emergence of a TC maximum at a specific length. The strong localization effect observed in NWs with high Ge concentration causes a considerable increase of TC contributed by the low-frequency ballistic phonons. Our results provide a better understanding of heat transport mechanisms in disordered quasi-one-dimensional materials and provide insight into controlling heat flow through the Anderson localization of phonons.

II. METHOD

Figure 1 provides a schematic representation of the NW structures in the NEGF calculations. The cross-section size of the NW has dimensions of $6a \times 6a$, where $a = 0.543$ nm represents the lattice constant of Si. The structure consists of the left and right leads, along with a central scattering region. The left and right leads are composed of pure silicon and have a length of $2a$, while the central scattering region comprises SiGe alloy NWs with lengths ranging from 0.5 to 2000 nm. To simplify the calculations, we only consider the mass differences (Si: 28.08 amu; Ge: 72.64 amu) in SiGe alloys and utilize the lattice constant and the force constants of Si for both atom types. Such simplifications are justified by the similarity of lattice parameters and interatomic potential parameters between Si and Ge in the Tersoff potential adopted throughout this paper. Similar simplifications have also been considered in previous studies [33,46–50]. Notably, it has been observed that small lattice mismatches have a minimal impact on phonon transmission [51]. While these simplifications may introduce minor changes to the phonon transmission spectra and TC, they do not affect the overall trends observed with variations in sample length and Ge concentration. This is due to the significant mass mismatch between Si and Ge, which results in mass scattering playing a dominant role in the overall scattering process. As the distribution of Ge atoms is random, we generated three

configurations of SiGe alloys, and the results are averaged across these configurations.

The NEGF method was originally developed to study electron transport [52], and it was extended to investigate phonon transport by Mingo *et al.* [43] and Zhang *et al.* [45]. In Si$_{1-x}$Ge$_x$ NWs, mass disorder is considered the primary scattering mechanism [25]. As a result, we neglected anharmonicity and focused mainly on discussing heat transport resulting from elastic scattering. In the NEGF approach, the atomic motion within the system is completely determined by the mass-normalized force constant matrix **K**. The force constant matrix $\bar{K}$ is calculated based on the second derivative of the potential energy U:

$$\mathbf{K}_{ij} = \frac{\bar{\mathbf{K}}}{\sqrt{M_i M_j}} = \frac{1}{\sqrt{M_i M_j}} \frac{\partial^2 U}{\partial u_i \partial u_j}, \qquad (1)$$

where the subscripts i and j represent degrees of freedom, and M is the atomic mass.

The total retarded Green's function of the central scattering region is defined as [44,45]

$$\mathbf{G}^r = \mathbf{G}^{CC} = \left[(\omega + i\eta)^2 \mathbf{I} - \mathbf{K}^C - \Sigma_L^r - \Sigma_R^r\right]^{-1}, \qquad (2)$$

where **I** is the identity matrix, ω denotes the frequency, η is a small positive real number, and $\mathbf{K}^C$ denotes the force constant matrix of the central scattering region. Here, $\sum_L^r$ and $\sum_R^r$ correspond to the retarded self-energies of the left and right leads, respectively. The self-energies are defined in terms of the uncoupled contact Green's functions of the respective leads $g_{L(R)}^r$:

$$\Sigma_{L(R)}^r = \mathbf{V}^{CL(R)} \mathbf{g}_{L(R)}^r \mathbf{V}^{L(R)C}, \qquad (3)$$

where $\mathbf{V}^{CL(R)}$ and $\mathbf{V}^{L(R)C}$ represent the coupling matrices between the left/right lead and the central region, and they are complex conjugate each other. The uncoupled contact Green's function of the left and right leads is defined as

$$\mathbf{g}_{L(R)}^r = [(\omega + i\eta)^2 \mathbf{I} - \mathbf{K}^{L(R)}]. \qquad (4)$$

According to the single-particle NEGF method [53], the transmission function of the device is expressed as

$$T(\omega) = \mathrm{Tr}(\mathbf{G}^r \mathbf{\Gamma}_L \mathbf{G}^a \mathbf{\Gamma}_R). \qquad (5)$$

The advanced Green's function in the central scattering region is the complex conjugate of the retarded Green's function, i.e., $\mathbf{G}^a = (\mathbf{G}^r)^\dagger$. Here, $\mathbf{\Gamma}_\alpha (\alpha = L, R)$ is the imaginary part of the self-energies and represents the broadening function of the left and right leads:

$$\mathbf{\Gamma}_\alpha = i(\Sigma_\alpha^r - \Sigma_\alpha^a) = -2\mathrm{Im}\mathbf{V}^{C\alpha} \mathbf{g}_\alpha^r \mathbf{V}^{\alpha C}. \qquad (6)$$

With the obtained transmission function, the thermal conductance can be obtained according to the Landauer transport theory [54–56]:

$$\sigma = \int_0^\infty \frac{\hbar\omega}{2\pi} \tau(\omega) \frac{\partial f_{BE}(\omega)}{\partial T} d\omega, \qquad (7)$$

$$f_{BE}(\omega) = [\exp(\hbar\omega/k_B T) - 1]^{-1}, \qquad (8)$$

where $f_{BE}(\omega)$ is the Bose-Einstein distribution function. Then the TC can be calculated by

$$\kappa = \frac{\sigma S}{L}. \qquad (9)$$
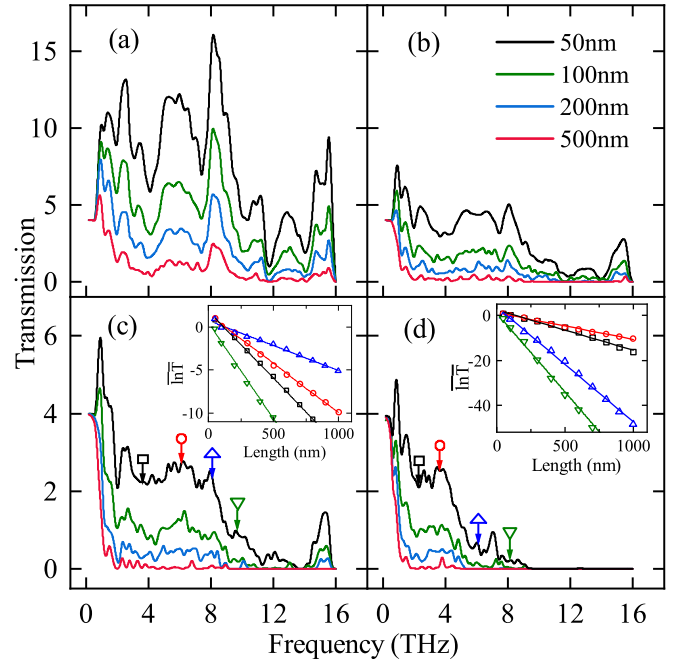
FIG. 2. Phonon transmission spectra of Si$_{1-x}$Ge$_x$ nanowires (NWs) with length ranging from 50 to 500 nm and different Ge concentration x. (a) $x = 0.01$, (b) $x = 0.05$, (c) $x = 0.1$, and (d) $x = 0.5$. Inset: Configuration averaged logarithm of transmission ($\ln \overline{T}$) as a function of length for the frequencies indicated by arrows in (c) and (d). Solid lines correspond to linear fits, which provide the localization lengths.

Here, S and L are the cross-sectional area and the length of the central scattering region, respectively.

III. RESULTS AND DISCUSSIONS

We first obtained the phonon transmission spectral of Si$_{1-x}$Ge$_x$ NWs with various lengths and Ge concentrations. Figure 2 presents the phonon transmission functions of Si$_{1-x}$Ge$_x$ NWs with varying lengths from 50 to 500 nm and various Ge concentrations. Since the TC of SiGe alloys has a U-shaped distribution with Ge concentration, we selected specific Ge concentrations with different characters: 1 and 5% with significant TC variation and 10 and 50% with large disorder but small TC variation. In general, the transmission decreases as the sample length increases due to enhanced isotope scattering. It is evident that the scattering strength intensifies with increasing Ge concentration, resulting in a significant reduction in transmission at the same lengths. However, for the low-frequency phonons (typically < 1 THz), the transmission remains nearly constant with increasing length, suggesting ballistic transport for those phonons. Nevertheless, this ballistic transport weakens as the Ge concentration rises. The frequency range supporting ballistic transport becomes narrower in heavily alloyed NWs, particularly for Si$_{0.5}$Ge$_{0.5}$ NWs. Additionally, the inset in Fig. 2 demonstrates that the phonon transmission of Si$_{1-x}$Ge$_x$ NWs at mid and high frequencies exhibits an exponential decay with increasing length, indicative of phonon localization
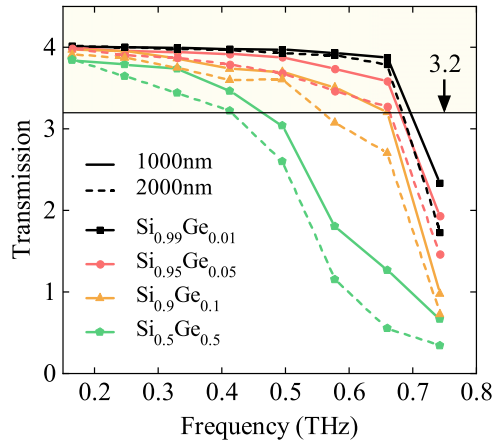
FIG. 3. Phonon transmission spectra < 0.74 THz for $Si_{1-x}Ge_x$ nanowires (NWs) with different Ge concentrations. The spectra correspond to NW lengths of 1 and 2 μm. The horizontal line at 3.2 represents the threshold between ballistic and diffusive transport, corresponding to 80% of the fully ballistic transmission value of 4.

[31]. Notably, this phenomenon becomes more pronounced with higher Ge concentrations.

To explore the behavior of ballistic transport at low frequencies, we conducted calculations on the phonon transmission spectra < 1 THz for $Si_{1-x}Ge_x$ NWs with lengths up to 2 μm. This allows us to examine whether these phonons can still maintain ballistic transport in $Si_{1-x}Ge_x$ NWs with micron length and with varying Ge concentrations. The corresponding results are shown in Fig. 3. To quantitatively assess the ballistic transport, we define that the phonons with $< 20\%$ decrease in transmission are considered ballistic [33]. The threshold for ballistic transport is subjectively defined, and altering it will not impact the key findings of our analysis. For NWs, there are four acoustic branches; thus, pure ballistic transmission at low frequencies corresponds to a value of four. It can be observed in Fig. 3 that, at low Ge concentration (1%), the transmission only exhibits slight decrease as the sample length increases from 1 to 2 μm, indicating strong ballistic transport behavior. Particularly, the transmission < 0.66 THz remains nearly unchanged, implying that these phonons can travel up to 2 μm without being scattered. As the Ge concentration increases, the transmission decreases, and the disparity between the transmission of 1 and 2 μm samples becomes more pronounced, which is a signature of enhanced phonon scattering. However, when the Ge concentration is between 5 and 10%, phonons with frequency < 0.49 THz still maintain ballistic transport in NWs with a 2 μm length. With a Ge concentration of 50%, the transmission between 0.41 and 0.74 THz significantly diminishes compared with other concentrations, which indicates that those modes in $Si_{0.5}Ge_{0.5}$ NWs exhibit diffusive transport. Nonetheless, the transmission of phonons < 0.41 THz still maintain ballistic transport even in NWs with a 2 μm length. Although the upper frequency bound for ballistic transport shifts toward lower frequencies as the Ge concentration increases, the contribution to the TC of the corresponding ballistic transport phonons increases, which will be described in detail later.
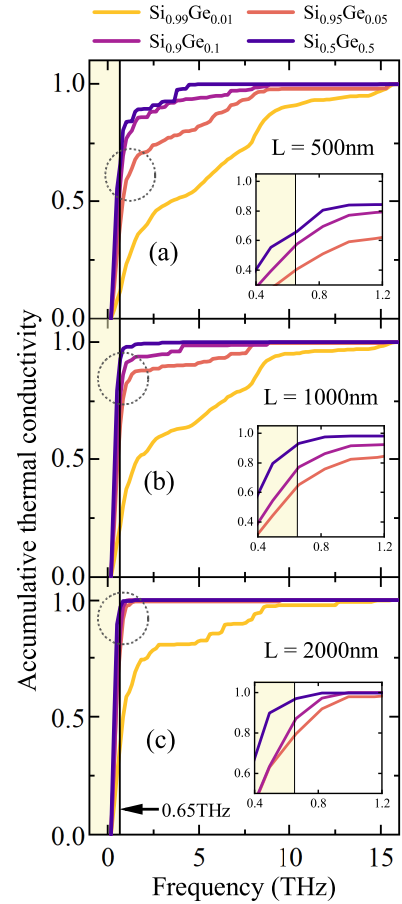
FIG. 4. Normalized thermal conductivity accumulations vs frequency for $Si_{1-x}Ge_x$ nanowires (NWs) with lengths of (a) 500 nm, (b) 1000 nm, and (c) 2000 nm. The insets provide enlarged diagrams of the curves within the dotted circle of each panel.

To illustrate the contribution of phonons at different frequencies to the total TC, we calculated the cumulative TC of $Si_{1-x}Ge_x$ NWs with length of 500, 1000, and 2000 nm based on their corresponding transmission spectra. The results are demonstrated in Fig. 4, where the cumulative TC is normalized by the total TC. For NWs with a length of 500 nm, when the Ge concentration is 1%, all phonons across the entire frequency range make a significant contribution to the total TC. However, as the Ge concentration increases, the contribution of high-frequency modes to TC reduces significantly. In Fig. 4, the vertical line represents $\omega/2\pi = 0.65$ THz, indicating the relative percentage of TC contributed by the modes below this frequency. The frequency 0.65 THz was selected for the analysis based on the observation that, below this frequency, there are only four acoustic modes of NWs present at each frequency. However, beyond this frequency, folded modes appear, which are more prone to scattering. For $Si_{0.99}Ge_{0.01}$ NWs with a length of 500 nm, the TC contributed by the modes < 0.65 THz is 12%. This value increases to 41, 58, and 66% as the Ge concentration is increased to 5, 10, and 50%, respectively. At higher Ge concentrations, the high-frequency modes have almost no contribution to the total TC, resulting in a flat cumulative TC curve beyond 10 THz. As the length of NWs increases, the contribution of
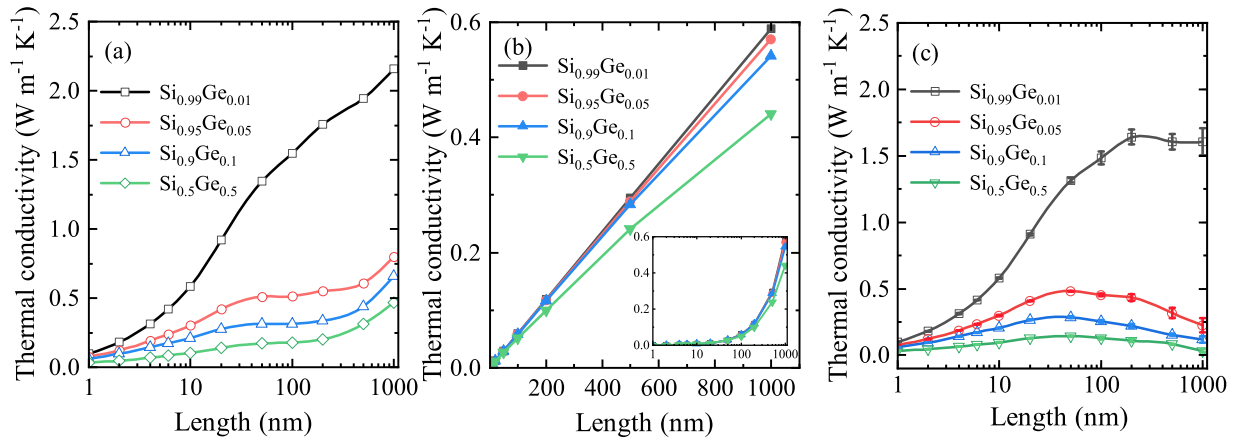
FIG. 5. (a) Total thermal conductivity (TC) of $Si_{1-x}Ge_x$ nanowires (NWs) as a function of length at 300 K. (b) The TC contributed by low-frequency phonons (< 0.65 THz). The insert shows the same plot with a logarithm x axis. (c) TC contributed by mid- and high-frequency phonons (0.65–16 THz). The error bars are obtained as the standard deviation of the TC from three random configurations.

high-frequency modes to TC further reduces for the same Ge concentration. This reduction is attributed to the localization of these modes. For $Si_{1-x}Ge_x$ NWs with a length of 2000 nm [Fig. 4(c)], as the Ge concentration increases from 1 to 50%, the TC contributed by phonons < 0.65 THz increases from 39 to 97%. This is primarily due to mass disorder causing scattering and localization of the mid- and high-frequency phonons with relatively small wavelengths, thus significantly reducing their contribution to TC. However, mass defects do not affect low-frequency phonons because they have longer wavelengths. Therefore, increasing the Ge concentration enhances the contribution of low-frequency phonons to heat transport.

Interestingly, we observe several plateaus in the cumulative TC curve within the mid- and high-frequency ranges, which is a signature of the occurrence of phonon localization. Figure 4 demonstrates that, as the Ge concentration increases, the slope of the TC accumulation function gradually decreases in the 1–15 THz range, indicating a decrease in the contribution of mid- and high-frequency phonons to heat transport. In $Si_{0.5}Ge_{0.5}$ NWs with a length of 500 nm, localized modes are indicated by small plateaus at 1–5 THz. The presence of plateaus in the cumulative TC curves suggests that an increase in mass disorder promotes the localization of phonons. Interestingly, when the length is increased to 2 μm, plateaus appear in NWs with a low Ge concentration as 1%, as shown in Fig. 4(c). Furthermore, these plateaus occur within a wider frequency range of 2.8–12.5 THz, with each plateau exhibiting a substantially increased width compared with those in shorter NWs.

To further elucidate the contribution of ballistic and localized phonons to TC at different lengths, we display the total TC, TC from modes < 0.65 THz and TC from modes beyond 0.65 THz as a function of length in Fig. 5. As shown in Fig. 5(a), the total TC increases with length for all Ge concentrations. The $Si_{0.99}Ge_{0.01}$ NWs exhibit a larger slope with length compared with those of the other three concentrations, resulting in relatively high TC values for long samples. In NWs with Ge concentration of 5, 10, and 50%, the TC increases linearly with length up to 20 nm, after which the slope

starts to decrease. Within the length range of 50 to 200 nm, the slope approaches zero. Beyond 200 nm, the slope of NWs with these three concentrations increases again, leading to a rapid TC increase with the elongation of samples.

To illustrate the slope changes in different length regions, we decompose the total TC into contributions from the low-frequency ballistic modes and the higher-frequency modes. To facilitate comparisons, we use a frequency of 0.65 THz as a threshold to separate ballistic and nonballistic modes. Figure 5(b) depicts that the TC contributed by phonons < 0.65 THz increases linearly with length, which is a characteristic of ballistic transport. For NWs with Ge concentration of 1, 5, and 10%, the TC contributed by modes < 0.65 THz remain nearly constant across different lengths considered. In $Si_{0.5}Ge_{0.5}$ NW, the slope of the TC curve for those modes slightly decreases with length, indicating some of the modes are slightly scattered. This is consistent with the transmission spectra shown in Fig. 3. For NWs with a length of 1000 nm, the phonons with frequencies < 0.65 THz contribute 21.84, 65.07, 77.12, and 92.92% to the total TC for Ge concentration of 1, 5, 10, and 50%, respectively. In Fig. 5(c), it can be observed that the TC contributed by the phonons beyond 0.65 THz initially increases and then decreases after reaching a maximum value at a certain length. This maximum TC is especially pronounced in NWs with Ge concentration $> 5\%$. The presence of this peak is an indication of phonon localization. For $Si_{0.99}Ge_{0.01}$ NWs, the peak TC occurs at a length of $\sim$200 nm, while for all other NWs, it takes place at $\sim$50 nm. Based on the above analysis, we can conclude that there is a competition between the ballistic transport of low-frequency modes and the localization of higher-frequency phonons. In NWs < 50 nm, ballistic phonon transport dominates heat transport, while in NWs > 50 nm, the localization of the high-frequency phonons starts to play an important role. In sample lengths between 50 and 200 nm, the reduction of TC caused by localization is comparable in magnitude with the enhancement of TC due to ballistic transport.

To quantitatively characterize diffusive transport and phonon localization, we calculated the phonon mean free
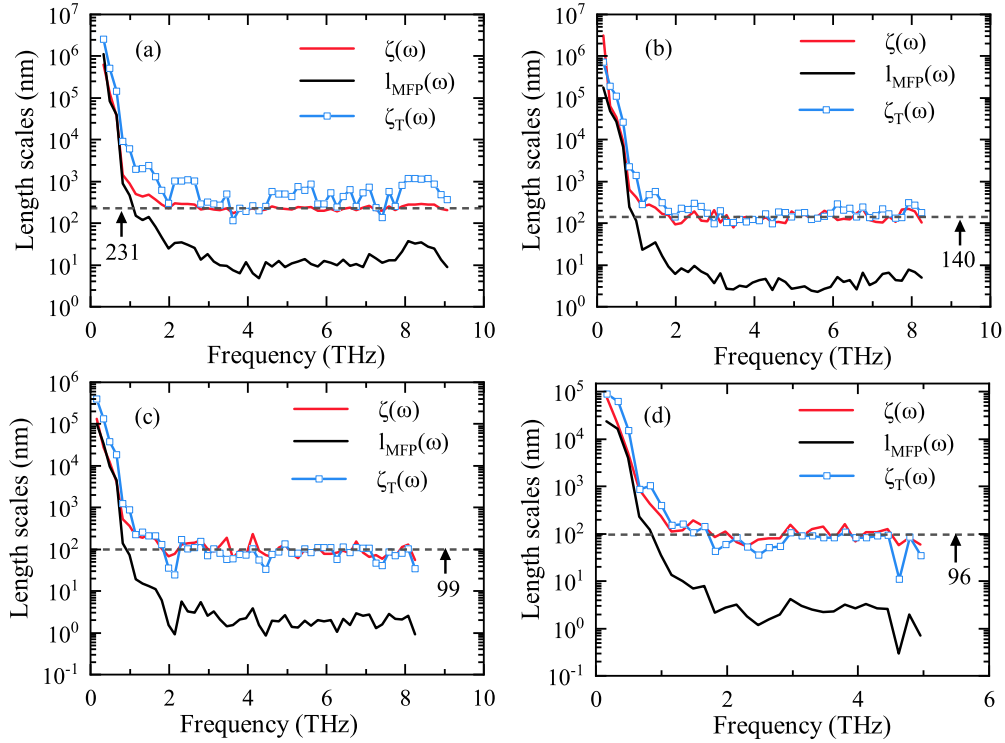
FIG. 6. Transport length scales vs frequency in $Si_{1-x}Ge_x$ nanowires (NWs) with x equals (a) 0.01, (b) 0.05, (c) 0.1, and (d) 0.5. The horizontal dashed lines indicate the averaged localization lengths beyond 2 THz.

path (l_{MFP}) and localization length (ζ) at different frequencies based on the length-dependent transmission spectra. The heat transport behavior of phonons is essentially determined by the relative magnitudes of the mean free path, localization length, and system length (L). When $L \ll l_{MFP}$, phonons transport ballistically. When the system size falls between l_{MFP} and ζ, i.e., $l_{MFP} \ll L \ll \zeta$, phonons transport diffusively, with the phonon mean free path as the characteristic length. The relationship between transmission $\tau(\omega)$, l_{MFP}, and L can be well described by [27,29] $\overline{\tau}(\omega) = N(\omega)/(L/l_{MFP} + 1)$, where $N(\omega)$ represents the number of phonon modes in a perfect Si NW. When $\zeta \ll L$, phonon localization happens, which is characterized by the localization length. The localization of phonons leads to an exponential decay in transmission. Similarly, the relationship among $T(\omega)$, L, and ζ can be described as $\overline{\ln T(\omega)} = -L/\zeta(\omega)$. By performing linear fitting of these two equations, we can obtain l_{MFP} and ζ of $Si_{1-x}Ge_x$ NWs at each frequency. In addition, the localization length is associated with the mean free path by the Thomas relation [57]: $\zeta_T \sim N l_{MFP}$. In a quasi-one-dimensional system, this relation can be used to verify the accuracy of the fitting results. It is worth noting that, since the localization length is much larger than the mean free path according to the Thomas relation, we fit l_{MFP} using the transmissions of short samples and fit ζ using the transmissions of long samples. Moreover, we only consider phonons with frequencies < 10 THz, as the transmissions beyond this range are close to zero and result in large fitting errors.

As show in Fig. 6, the mean free path of phonons < 1 THz is two or three orders of magnitude larger than the size of

the system we studied, consistent with the characteristics of ballistic transport. Both the mean free path and localization length of phonons at low frequencies decreases rapidly as the frequency increases. However, beyond 2 THz, l_{MFP} and ζ become almost frequency independent. For all Ge concentrations, l_{MFP} and ζ can be well described by the Thomas relation, i.e., the Thomas length closely approximates the localization length. The mean localization lengths >2 THz for Ge concentrations of 1, 5, 10, and 50% are 231, 140, 99, and 96 nm, respectively. Together with the cumulative TC analysis in Fig. 4, we find that, when the length of NWs is 5–10 times the localization length of a specific mode, plateaus appear in the cumulative TC curve at the corresponding frequency.

To investigate the localization effect across the entire frequency spectrum, we illustrate the color map of the normalized TC as a function of frequency and sample length in Fig. 7. The normalization of TC is done with respect to the corresponding maximum values at each frequency. For $Si_{1-x}Ge_x$ NWs with varying concentrations of Ge, we observe that the TC of the modes < 1 THz reaches its maximum at a length of 2000 nm, which is consistent with ballistic transport phenomenon. However, as the Ge concentration increases, the number of modes reaching the maximum TC at 2000 nm significantly decreases. In general, the length corresponding to the maximum TC decreases as frequency increases. Additionally, with higher Ge concentrations, the length of maximum TC decreases rapidly, especially at higher frequencies. This indicates an intensified localization effect. In general, high-frequency phonons are more prone to
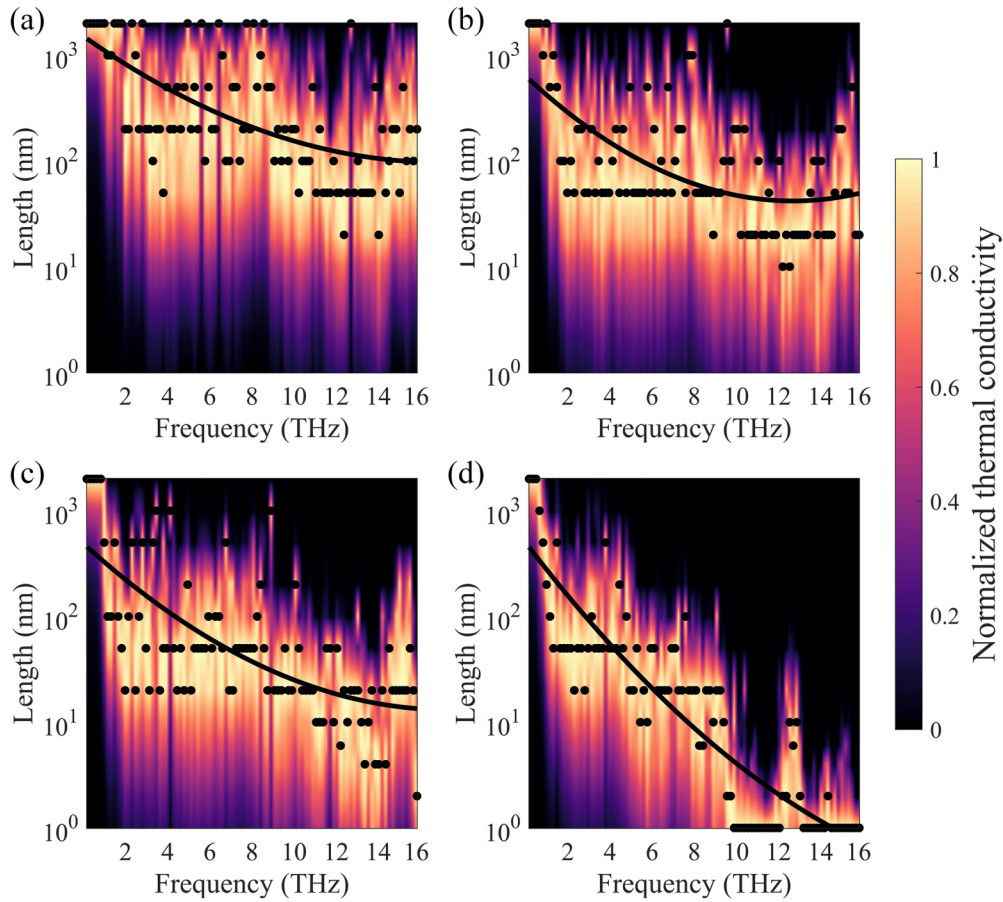
FIG. 7. Colormap of normalized thermal conductivity (TC) with the variation of frequencies and sample lengths for $Si_{1-x}Ge_x$ nanowires (NWs) at a temperature of 300 K. The Ge concentration x equals (a) 0.01, (b) 0.05, (c) 0.1, and (d) 0.5. The TC at each frequency is normalized by its respective maximum value for different sample lengths. The solid circles in the plots represent the maximum TC achieved at each frequency. To capture the trend, a quadratic fit of the maximum TC vs frequency is represented by the corresponding black solid line.

localization. As the Ge concentration increases, more phonons become localized, and the localization length gets shorter and shorter.

IV. CONCLUSIONS

In summary, we elucidate the transport behaviors of phonons in SiGe-alloyed NWs across different lengths and Ge concentrations. We found that the $Si_{1-x}Ge_x$-alloyed NWs exhibit ballistic transport for low-frequency phonons over a distance of at least 2 microns. As the Ge concentration increases, the upper frequency limit for ballistic transport shifts toward lower frequencies. However, despite this shift, the contribution of ballistic phonons to TC is increased significantly. Moreover, we have comprehensively confirmed the phenomenon of Anderson localization in SiGe-alloyed NWs through the exponential decay of transmission, the plateaus in accumulative TC curves, and the maximum TC observed with varying length. The localization length in SiGe-alloyed NWs decreases with an increase in both frequency and Ge concentration. Especially the localization length is particularly sensitive to the concentration of mass disorder, with high frequencies experiencing a fast decrease in localization length with increasing Ge concentration.

Our findings contribute to a deeper understanding of thermal transport in low-dimensional disordered materials and have potential implications for designing materials or structures with ultrahigh or ultralow TCs. Specifically, by strategically designing the composition, it is possible to manipulate the strength of phonon localization, which could be useful in thermoelectric energy conversion and heat dissipation. Additionally, by incorporating spatial-dependent localization strength into the structure design, thermal functional materials with improved performances could be achieved. In this paper, we focused on configurations with random Ge distributions based on harmonic force constants. In future research, it could be worthwhile to investigate Ge distributions with spatial correlations [58] as well as the effect of anharmonicity on localization.

[1] S. Xiong, K. Sääskilahti, Y. A. Kosevich, H. Han, D. Donadio, and S. Volz, Blocking Phonon Transport by Structural Resonances in Alloy-Based Nanophononic Metamaterials Leads to Ultralow Thermal Conductivity, Phys. Rev. Lett. **117**, 025503 (2016).

[2] W. Li, L. Lindsay, D. A. Broido, D. A. Stewart, and N. Mingo, Thermal conductivity of bulk and nanowire $Mg_2Si_xSn_{1-x}$ alloys from first principles, Phys. Rev. B **86**, 174307 (2012).

[3] Y. Zhou and M. Hu, Record low thermal conductivity of polycrystalline Si nanowire: Breaking the Casimir limit by severe suppression of propagons, Nano Lett. **16**, 6178 (2016).

[4] B. L. Davis, and M. I. Hussein, and Nanophononic Metamaterial: Thermal Conductivity Reduction by Local Resonance, Phys. Rev. Lett. **112**, 055505 (2014).

[5] R. Cheaito, J. C. Duda, T. E. Beechem, K. Hattar, J. F. Ihlefeld, D. L. Medlin, M. A. Rodriguez, M. J. Campion, E. S. Piekos, and P. E. Hopkins, Experimental Investigation of Size Effects on the Thermal Conductivity of Silicon-Germanium Alloy Thin Films, Phys. Rev. Lett. **109**, 195901 (2012).

[6] J. L. Braun, C. H. Baker, A. Giri, M. Elahi, K. Artyushkova, T. E. Beechem, P. M. Norris, Z. C. Leseman, J. T. Gaskins, and P. E. Hopkins, Size effects on the thermal conductivity of amorphous silicon thin films, Phys. Rev. B **93**, 140201(R) (2016).

[7] M. N. Luckyanova, J. Garg, K. Esfarjani, A. Jandl, M. T. Bulsara, A. J. Schmidt, A. J. Minnich, S. Chen, M. S. Dresselhaus, Z. Ren *et al.*, Coherent phonon heat conduction in superlattices, Science **338**, 936 (2012).

[8] J. Ravichandran, A. K. Yadav, R. Cheaito, P. B. Rossen, A. Soukiassian, S. J. Suresha, J. C. Duda, B. M. Foley, C. Lee, Y. Zhu *et al.*, Crossover from incoherent to coherent phonon scattering in epitaxial oxide superlattices, Nat. Mater. **13**, 168 (2014).

[9] P. Hołuj, C. Euler, B. Balke, U. Kolb, G. Fiedler, M. M. Müller, T. Jaeger, E. Chávez Angel, P. Kratzer, and G. Jakob, Reduced thermal conductivity of TiNiSn/HfNiSn superlattices, Phys. Rev. B **92**, 125436 (2015).

[10] B. Saha, Y. R. Koh, J. P. Feser, S. Sadasivam, T. S. Fisher, A. Shakouri, and T. D. Sands, Phonon wave effects in the thermal transport of epitaxial TiN/(Al,Sc)N metal/semiconductor superlattices, J. Appl. Phys. **121**, 015109 (2017).

[11] M. Maldovan, Narrow Low-Frequency Spectrum and Heat Management by Thermocrystals, Phys. Rev. Lett. **110**, 025902 (2013).

[12] N. Zen, T. A. Puurtinen, T. J. Isotalo, S. Chaudhuri, and I. J. Maasilta, Engineering thermal conductance using a two-dimensional phononic crystal, Nat. Commun. **5**, 3435 (2014).

[13] J. Maire, R. Anufriev, R. Yanagisawa, A. Ramiere, S. Volz, and M. Nomura, Heat conduction tuning by wave nature of phonons, Sci. Adv. **3**, e1700027 (2017).

[14] B. Liao and G. Chen, Nanocomposites for thermoelectrics and thermal engineering, MRS Bull. **40**, 746 (2015).

[15] A. Miura, S. Zhou, T. Nozaki, and J. Shiomi, Crystalline–amorphous silicon nanocomposites with reduced thermal conductivity for bulk thermoelectrics, ACS Appl. Mater. Interfaces **7**, 13484 (2015).

[16] Y. Zhou, Assessing the quantum effect in classical thermal conductivity of amorphous silicon, J. Appl. Phys. **129**, 235104 (2021).

[17] P. Sheng, *Introduction to Wave Scattering, Localization, and Mesoscopic Phenomena*, 2nd ed. (Springer, Berlin, New York, 2006).

[18] S. Datta, *Electronic Transport in Mesoscopic Systems* (Cambridge University Press, Cambridge, 1995).

[19] G. Chen, *Nanoscale Energy Transport and Conversion: A Parallel Treatment of Electrons, Molecules, Phonons, and Photons* (Oxford University Press, New York, 2005).

[20] H. Bao, J. Chen, X. Gu, and B. Cao, A review of simulation methods in micro/nanoscale heat conduction, ES Energy Environ. **1**, 16 (2018).

[21] P. B. Allen, J. L. Feldman, J. Fabian, and F. Wooten, Diffusons, locons and propagons: Character of atomie yibrations in amorphous Si, Philos. Mag. B **79**, 1715 (1999).

[22] N. W. Lundgren, G. Barbalinardo, and D. Donadio, Mode localization and suppressed heat transport in amorphous alloys, Phys. Rev. B **103**, 024204 (2021).

[23] R. T. Howie, I. B. Magdău, A. F. Goncharov, G. J. Ackland, and E. Gregoryanz, Phonon Localization by Mass Disorder in Dense Hydrogen-Deuterium Binary Alloy, Phys. Rev. Lett. **113**, 175501 (2014).

[24] I. B. Magdău and G. J. Ackland, Infrared Peak Splitting from Phonon Localization in Solid Hydrogen, Phys. Rev. Lett. **118**, 145701 (2017).

[25] H. Kim, I. Kim, H. Choi, and W. Kim, Thermal conductivities of $Si_{1-x}Ge_x$ nanowires with different germanium concentrations and diameters, Appl. Phys. Lett. **96**, 233106 (2010).

[26] D. Li, Y. Wu, R. Fan, P. Yang, and A. Majumdar, Thermal conductivity of Si/SiGe superlattice nanowires, Appl. Phys. Lett. **83**, 3186 (2003).

[27] I. Savić, N. Mingo, and D. A. Stewart, Phonon Transport in Isotope-Disordered Carbon and Boron-Nitride Nanotubes: Is Localization Observable? Phys. Rev. Lett. **101**, 165502 (2008).

[28] T. Yamamoto, K. Sasaoka, and S. Watanabe, Universality and Diversity in a Phonon-Transmission Histogram of Isotope-Disordered Carbon Nanotubes, Phys. Rev. Lett. **106**, 215503 (2011).

[29] J. Mendoza and G. Chen, Anderson localization of thermal phonons leads to a thermal conductivity maximum, Nano Lett. **16**, 7616 (2016).

[30] M. N. Luckyanova, J. Mendoza, H. Lu, B. Song, S. Huang, J. Zhou, M. Li, Y. Dong, H. Zhou, J. Garlow *et al.*, Phonon localization in heat conduction, Sci. Adv. **4**, eaat9460 (2018).

[31] Y. Guo, M. Bescond, Z. Zhang, S. Xiong, K. Hirakawa, M. Nomura, and S. Volz, Thermal conductivity minimum of graded superlattices due to phonon localization, APL Mater. **9**, 091104 (2021).

[32] T. Juntunen, O. Vänskä, and I. Tittonen, Anderson Localization Quenches Thermal Transport in Aperiodic Superlattices, Phys. Rev. Lett. **122**, 105901 (2019).

[33] R. Hu and Z. Tian, Direct observation of phonon Anderson localization in Si/Ge aperiodic superlattices, Phys. Rev. B **103**, 045304 (2021).

[34] Z. Zhang and J. Chen, Thermal conductivity of nanowires, Chin. Phys. B **27**, 035101 (2018).

[35] L. Yang, R. Prasher, and D. Li, From nanowires to super heat conductors, J. Appl. Phys. **130**, 220901 (2021).

[36] C. W. Chang, D. Okawa, H. Garcia, A. Majumdar, and A. Zettl, Breakdown of Fourier's Law in Nanotube Thermal Conductors, Phys. Rev. Lett. **101**, 075903 (2008).

[37] G. Zhang and B. Li, Thermal conductivity of nanotubes revisited: Effects of chirality, isotope impurity, tube length, and temperature, J. Chem. Phys. **123**, 114714 (2005).

[38] J. Shiomi and S. Maruyama, Molecular dynamics of diffusive-ballistic heat conduction in single-walled carbon nanotubes, Jpn. J. Appl. Phys. **47**, 2005 (2008).

[39] N. Yang, G. Zhang, and B. Li, Violation of Fourier's law and anomalous heat diffusion in silicon nanowires, Nano Today **5**, 85 (2010).

[40] G. Xie, Y. Guo, X. Wei, K. Zhang, L. Sun, J. Zhong, G. Zhang, and Y.-W. Zhang, Phonon mean free path spectrum and thermal conductivity for $Si_{1-x}Ge_x$ nanowires, Appl. Phys. Lett. **104**, 233901 (2014).

[41] T.-K. Hsiao, H.-K. Chang, S.-C. Liou, M.-W. Chu, S.-C. Lee, and C.-W. Chang, Observation of room-temperature ballistic thermal conduction persisting over 8.3 μm in SiGe nanowires, Nat. Nanotechnol. **8**, 534 (2013).

[42] B. Smith, G. Fleming, K. D. Parrish, F. Wen, E. Fleming, K. Jarvis, E. Tutuc, A. J. H. McGaughey, and L. Shi, Mean free path suppression of low-frequency phonons in SiGe nanowires, Nano Lett. **20**, 8384 (2020).

[43] N. Mingo and L. Yang, Phonon transport in nanowires coated with an amorphous material: An atomistic Green's function approach, Phys. Rev. B **68**, 245406 (2003).

[44] T. Yamamoto and K. Watanabe, Nonequilibrium Green's Function Approach to Phonon Transport in Defective Carbon Nanotubes, Phys. Rev. Lett. **96**, 255503 (2006).

[45] W. Zhang, T. S. Fisher, and N. Mingo, Simulation of interfacial phonon transport in Si-Ge heterostructures using an atomistic Green's function method, J. Heat Transf. **129**, 483 (2007).

[46] B. Latour, N. Shulumba, and A. J. Minnich, *Ab initio* study of mode-resolved phonon transmission at Si/Ge interfaces using atomistic Green's functions, Phys. Rev. B **96**, 104310 (2017).

[47] Z. Tian, K. Esfarjani, and G. Chen, Enhancing phonon transmission across a Si/Ge interface by atomic roughness: First-principles study with the Green's function method, Phys. Rev. B **86**, 235304 (2012).

[48] Y. Guo, M. Bescond, Z. Zhang, M. Luisier, M. Nomura, and S. Volz, Quantum mechanical modeling of anharmonic phonon-phonon scattering in nanostructures, Phys. Rev. B **102**, 195412 (2020).

[49] R. Hu and Z. Tian, Thermal interface doping strategies based on Bayesian optimization, Surf. Interfaces **30**, 101847 (2022).

[50] J. Dai and Z. Tian, Rigorous formalism of anharmonic atomistic green's function for three-dimensional interfaces, Phys. Rev. B **101**, 041301(R) (2020).

[51] X. Li and R. Yang, Effect of lattice mismatch on phonon transmission and interface thermal conductance across dissimilar material interfaces, Phys. Rev. B **86**, 054305 (2012).

[52] L. V. Keldysh, Ionization in the field of a strong eletromagnetic wave, J. Exptl. Theoret. Phys. (USSR) **47**, 1945 (1964) [Sov. Phys. JETP **20**, 1307 (1965)].

[53] Y. Meir and N. S. Wingreen, Landauer Formula for the Current Through an Interacting Electron Region, Phys. Rev. Lett. **68**, 2512 (1992).

[54] R. Landauer, Spatial variation of currents and fields due to localized scatterers in metallic conduction, IBM J. Res. Dev. **1**, 223 (1957).

[55] R. Landauer, Electrical resistance of disordered one-dimensional lattices, Philos. Mag. (1798–1977) **21**, 863 (1970).

[56] Y. Imry and R. Landauer, Conductance viewed as transmission, Rev. Mod. Phys. **71**, S306 (1999).

[57] D. J. Thouless, Maximum Metallic Resistance in Thin Wires, Phys. Rev. Lett. **39**, 1167 (1977).

[58] S. Thébaud, L. Lindsay, and T. Berlijn, Breaking Rayleigh's Law with Spatially Correlated Disorder to Control Phonon Transport, Phys. Rev. Lett. **131**, 026301 (2023).